

This is the post-print version of the following article: *Tomás-Loba, A; Manieri, E; González-Terán, B; Mora, A; Leiva-Vega, L; Santamans, AM; Romero-Becerra, R; Rodríguez, E; Pintor-Chocano, A; Feixas, F; López, JA; Caballero, B; Trakala, M; Blanco, Ó; Torres, JL; Hernández-Cosido, L; Montalvo-Romeral, V; Matesanz, N; Roche-Molina, M; Bernal, JA; Mischo, H; León, M; Caballero, A; Miranda-Saavedra, D; Ruiz-Cabello, J; Nevzorova, YA; Cubero, FJ; Bravo, J; Vázquez, J; Malumbres, M; Marcos, M; Osuna, S; Sabio, G.* [p38 gamma is essential for cell cycle progression and liver tumorigenesis](#). *Nature* **2019**, 568, 557-560

DOI: [10.1038/s41586-019-1112-8](https://doi.org/10.1038/s41586-019-1112-8)

This article may be used for non-commercial purposes in accordance with Nature Terms and Conditions for Self-Archiving.

p38gamma is essential for cell cycle progression and liver tumourigenesis

Antonia Tomás-Loba¹, Elisa Manieri^{1,2#}, Bárbara González-Terán^{1#}, Alfonso Mora¹, Luis Leiva-Vega¹, Ayelén M. Santamans¹, Rafael Romero-Becerra¹, Elena Rodríguez¹, Aránzazu Pintor-Chocano¹, Ferran Feixas³, Juan Antonio López^{1,15}, Beatriz Caballero¹, Marianna Trakala⁴, Óscar Blanco⁵, Jorge L. Torres⁵, Lourdes Hernández-Cosido⁵, Valle Montalvo-Romeral¹, Nuria Matesanz¹, Marta Roche-Molina¹, Juan Antonio Bernal¹, Hannah Mischo⁶, Marta León¹, Ainoa Caballero¹, Diego Miranda-Saavedra^{7,8}, Jesús Ruiz-Cabello^{1,9,10}, Yulia A. Nevzorova^{10,11}, Francisco Javier Cubero^{12,13}, Jerónimo Bravo¹⁴, Jesús Vázquez^{1,15}, Marcos Malumbres⁴, Miguel Marcos⁵, Sílvia Osuna^{3,16}, Guadalupe Sabio^{1*}

1. Centro Nacional de Investigaciones Cardiovasculares (CNIC), Madrid, Spain.
2. Centro Nacional de Biotecnología, CSIC, Madrid, Spain.
3. Departament de Química and Institut de Química Computacional i Catalisi, Universitat de Girona, Spain.
4. Centro Nacional de Investigaciones Oncológicas (CNIO), Madrid, Spain.
5. University of Salamanca, University Hospital of Salamanca-IBSAL, Salamanca, Spain.
6. Sir William Dunn School of Pathology, Oxford University, Oxford, UK.
7. Centro de Biología Molecular Severo Ochoa, CSIC/Universidad Autónoma de Madrid, Madrid, Spain.
8. University of Oxford Wolfson Building, Parks Road, Oxford, UK.

9. CIC biomaGUNE, 2014, Donostia-San Sebastián, Spain; IKERBASQUE, Basque Foundation for Science, Spain; Ciber de Enfermedades Respiratorias (CIBERES), Madrid, Spain.
10. University Hospital RWTH Aachen, Aachen, Germany.
11. Faculty of Biology, Complutense University, Madrid, Spain.
12. Complutense University School of Medicine, Madrid, Spain.
13. 12 de Octubre Health Research Institute (imas12), Madrid. Spain.
14. Instituto de Biomedicina de Valencia, IBV-CSIC, Valencia, Spain.
15. CIBER Enfermedades Cardiovasculares (CIBERCV), Madrid, Spain.
16. ICREA, Barcelona, Spain.

Equal contribution

*To whom correspondence should be addressed:

Guadalupe Sabio, DVM, PhD.

Assistant Professor

Centro Nacional de Investigaciones Cardiovasculares

C/ Melchor Fernández Almagro, 3

28029 Madrid (Spain)

tel.: (34) 91453 12 00 ext 2004

The cell cycle is a tightly regulated process controlled by the conserved cyclin-dependent kinase (CDK)–cyclin protein complex¹. However, control of the G0/G1 transition remains incompletely understood. Here, we demonstrate that p38 mitogen-activated protein kinase (MAPK) gamma (p38 γ) acts as a CDK-like kinase and thus cooperates with CDKs, regulating entry into the cell cycle and sharing high sequence homology, inhibition sensitivity, and substrate specificity with CDK family members. In hepatocytes, p38 γ induces proliferation after partial hepatectomy (PHx) by promoting Rb phosphorylation on known CDK target residues. Lack of p38 γ or treatment with the p38 γ inhibitor pirfenidone protects against chemically-induced liver tumour formation. Furthermore, human hepatocellular carcinoma (HCC) biopsies show high p38 γ expression, suggesting p38 γ as a potential target for HCC therapy.

Despite the identified role of CDKs in cell cycle progression, the precise molecular mechanisms that trigger cell cycle initiation are unknown in most cell types. The p38MAPKs (p38 α , β , γ and δ) and the CDKs belong to the CMGC protein kinase superfamily². Sequence analysis of catalytic domains shows that the p38 MAPKs form a sister group within the CDK family (**Extended data Fig. 1a**). A heuristic three-dimensional (3D) search of active CDK1/2 highlighted a higher degree of structural similarity with p38 γ than with other stress kinases (**Supplementary Table 1**). Molecular dynamics (MD) simulations revealed a similar affinity of the CDK1 inhibitor RO3306 for the ATP-binding sites of p38 γ and CDK1 stronger than for CDK2 or p38 δ , with no affinity towards p38 α . This suggests that p38 γ and CDK share similar inhibition mechanisms (**Extended data Fig. 1b-e, and videos 1, 2**).

To test whether these kinases share common substrates, we studied retinoblastoma tumour suppressor protein (Rb). Rb remains hypophosphorylated and active in G₀, but during cell cycle progression it is sequentially phosphorylated by CDKs, leading to its inactivation promoting cell cycle entry and proliferation³. *In vitro* kinase assays revealed that p38 γ equally phosphorylates Rb at twelve CDK target residues³ (**Extended data Fig. 1f, 2a**). Moreover, we detected Rb in immunoprecipitates of p38 γ in liver lysates (**Fig. 1a**). p38 γ -mediated Rb phosphorylation *in vivo* was confirmed in liver from p38 γ ^{-/-} (p38 γ KO) mice infected with liver-specific adeno-associated viruses expressing a constitutively active form of p38 γ (AAVp38 γ *) (**Fig. 1b**). These data indicate that p38 γ presents similarities with CDKs, sharing structural homology, comparable binding dynamics for RO3306 in the ATP-binding site, and a similar substrate specificity.

Phosphorylation-induced Rb inactivation in hepatocytes is sufficient to promote G₀/G₁ transition^{4,5}. After PHx, a well-established model of hepatocyte proliferation, p38 γ was phosphorylated and activated (**Fig. 1c**). To address the physiological impact of p38 γ -mediated Rb phosphorylation after PHx, we compared hepatocyte proliferation in mice lacking p38 γ in hepatocytes (AlbCRE-p38 γ mice) and in control AlbCRE mice (AlbCRE^{+/-}). Whereas PHx induced Rb phosphorylation in control mice, this effect was abolished in AlbCRE-p38 γ mice (**Fig. 1d**) without changes in CDK expression (**Extended data Fig. 2b**). Loss of Rb phosphorylation in AlbCRE-p38 γ mice correlated with lower induction of cyclin E and A (**Extended data Fig. 2b**). Compared with AlbCRE mice, AlbCRE-p38 γ mice also showed markedly reduced hepatic DNA synthesis and hepatocyte proliferation, measured by BrdU incorporation, Ki67-immunostaining and PCNA expression (**Fig. 1e-g**). The lower hepatocyte proliferation in AlbCRE-p38 γ mice was reflected in lower liver regeneration (**Fig. 1h Extended data**

Fig. 3a). Together, these results indicate that p38 γ is required in hepatocytes for Rb phosphorylation and liver regeneration.

To corroborate these results and avoid the effects of unspecific deletion of p38 γ , we infected AlbCRE-p38 γ with AAVp38 γ^* . The hepatocyte-specific expression of active p38 γ recovered hepatocyte proliferation, Rb phosphorylation, and liver regeneration **(Extended data Fig. 3 b-f)**. N-terminal Rb phosphorylation by p38 α delays cell-cycle progression, rendering Rb insensitive to CDK regulation⁶. Unlike hepatocyte-specific active p38 α , active p38 γ promoted phosphorylation of the Rb C terminus and hepatocyte proliferation **(Extended data Fig. 3g-h)**.

Lack of p38 γ impaired liver regeneration although did not affect survival **(Extended data Fig. 4a)**. This is consistent with peak Rb phosphorylation and hepatocyte proliferation, which occurred at 60h post PHx **(Extended data Fig. 4b and 4f)**. p38 δ , the p38 isoform most closely related to p38 γ , can compensate the lack of p38 γ and phosphorylate its substrates⁷⁻⁹. p38 δ expression increased in AlbCRE-p38 γ mice after PHx **(Extended data Fig. 4c)**, and the lack of both kinases in hepatocytes (AlbCRE-p38 $\gamma\delta$) abolished Rb phosphorylation and significantly delayed hepatocyte proliferation **(Extended data Fig. 4d-h)**.

Stress-activated p38 γ -mediated cell cycle regulation is not restricted to hepatocytes since p38 γ also phosphorylates Rb in gut epithelial cells treated with dextran sulfate sodium **(Extended data Fig. 5)**.

The precise mechanism by which Rb is phosphorylated *in vivo* remains unclear because single genetic ablation of CDK2 or CDK1 does not block hepatocyte DNA replication during liver regeneration^{10,11}. *In vitro* kinase assays with CDK2 and p38 γ^* showed that

more Rb residues were phosphorylated when both kinases were used, suggesting that these kinases work in concert to control Rb phosphorylation (**Extended data Fig. 6a**). Immunoprecipitation analysis confirmed interaction between p38 γ and CDK2 in hepatocytes (**Extended data Fig. 6b-c**). To explore the cooperation between p38 γ and CDK2, we examined the kinase activation after PHx. p38 γ was activated just 4 hours after PHx, increasing its binding and the phosphorylation of Rb at Ser795 and Ser821/826. Moreover, a second p38 γ activation peak was detected after 24 hours with Rb phosphorylation on residues Ser807/811 and Ser780, preceding the proliferation detected by BrdU incorporation (**Fig. 2a and Extended data Fig. 6d**). Interaction between CDK2 and p38 γ increased during these two p38 γ activation peaks (**Fig. 2a**). These results correlate with a stronger interaction between CDK1/2 and Rb when p38 γ is present (**Extended data Fig. 6e**), whereas p38 γ binding to Rb was independent of CDK1/2 (**Extended data Fig. 6c**). Moreover, studies with a nonphosphorylatable Rb mutant¹² indicated that Rb phosphorylation is required for its binding to CDK2 (**Extended data Fig. 6f**).

In addition, p38 γ was able to compensate the loss of CDK1 or CDK2 as infection with AAVp38 γ * rescued Rb phosphorylation after CDK1/2 silencing or ablation and fully preserved hepatocyte proliferation and hepatic DNA synthesis in the livers of CDK1/2-depleted mice (**Fig. 2b-d and Extended data Fig. 6g-i**). Collectively, these results suggest that p38 γ controls hepatocyte proliferation through the regulation of Rb phosphorylation and likely induces proliferation through cooperation with classical CDKs. Moreover, infection with AAVp38 γ * rescued Rb phosphorylation and proliferation after silencing of CDK4 and CDK6 (**Extended data Fig. 6j-m**), confirming the ability of p38 γ to phosphorylate Rb in the absence of these CDKs.

CDK1 ablation protects against liver tumourigenesis¹³. Interestingly, there are similar CDK1 and p38 γ mutation rates in human HCC samples (**Extended data Fig. 7a**) and the mutations located in the L16 loop of p38 γ induce its activation¹⁴. Moreover, p38 γ expression was higher in human HCC cell lines than in primary hepatocytes (**Extended data Fig. 7b**) and was activated in liver from genetically engineered HCC mouse models (**Extended data Fig. 7c**). Most importantly, p38 γ staining was far stronger in human HCC biopsies than in non-tumour tissues (**Fig. 3a and Extended data Fig. 7d**). In addition, p38 γ expression directly correlated with actin and collagen (*colla*), markers of fibrosis that usually precede the development of liver cancer (**Fig. 3b and Supplementary Table 2**); moreover, high p38 γ expression was associated with worse outcome in liver cancer (**Fig. 3c**). In agreement, p38 γ knockdown attenuated proliferation and colony formation in the HCC cell lines (**Extended data Fig. 8**). These findings may indicate an involvement of p38 γ in human liver tumour development.

In agreement, p38 γ was activated after DEN injection and its deficiency markedly attenuated DEN-induced Rb phosphorylation and compensatory proliferation, correlating with lower PCNA expression and hepatocytes proliferation (**Extended data Fig. 9a-c**). Moreover, HCC was strongly suppressed in AlbCRE-p38 γ mice, which had smaller and fewer tumours and improved survival than AlbCRE mice (**Fig. 3d-g**).

AlbCRE-p38 γ mice were also protected against carbon tetrachloride (CCl₄)- and streptozotocin (STZ)/HFD-induced liver cancer (**Extended data Fig. 9d-g**). We next evaluated the effect on liver tumourigenesis of p38 γ inactivation. The inhibitor pirfenidone bound to and inhibited p38 γ without affecting CDK2 activity (**Fig. 4a and Extended data Fig. 10a-b**), and reduced hepatic DNA synthesis in WT mice but not in AlbCRE-p38 γ mice, indicating a p38 γ -mediated effect (**Fig. 4b**). Without evident

secondary effects, pirfenidone reduce the number and size of liver tumours in DEN-treated mice and improved its survival (**Fig. 4c-e and Extended data Fig. 10c**). Moreover, specific ablation of p38 γ using AAV2/8-CAG-Cre once the tumours were already established confirmed the therapeutic effects of p38 γ inhibition (**Extended data Fig. 10d-g**). Interestingly, those tumours that grow in the pirfenidone-treated mice had lost Rb expression (**Fig. 4f**), suggesting that upon pirfenidone treatment only tumours lacking Rb are able to proliferate. These data are consistent with the inactivation of tumor suppressors such as Rb through chromosomal mutations during tumour development¹⁵, thus indicating that pirfenidone will be effective against HCC tumours that maintain Rb expression.

Our results show that p38 γ MAPK functions as a CDK-collaborating protein; similarly to the role of MAPK in CDK signaling recently established in yeast¹⁶. p38 MAPK protein family members fall into two categories: p38 α and p38 β on one hand and p38 γ and p38 δ on the other¹⁷. All members share the same mechanism of activation by upstream MAPK kinases; however, the two p38 classes do not share substrate specificity or inhibitor selectivity. p38 α increases cell survival by N-terminal phosphorylation of Rb, which renders Rb insensitive to inactivation by CDKs⁶. Consequently, p38 α deletion in hepatocytes results in increased HCC development¹⁸. These results reinforce the idea that different p38s can have opposing functions¹⁹.

We demonstrated that p38 γ is sufficient to induce cell cycle entry even when CDKs expression is downregulated. This might allow a cell cycle regulation different from the canonical mitogenic signal/CDK activation pathway, via stress damage/p38 γ activation, thereby exerting tight regulation on the cell cycle.

This study suggests that a non-classical CDK could initiate the cell cycle in a cyclin

independent manner in quiescence, when CDK/cyclin complexes are less abundant. p38 γ may represent a unique kinase that enables cells to escape from quiescence in response to stress stimuli. The confirmation that p38 γ is essential for Rb-dependent cell cycle progression and liver tumourigenesis strongly supports the potential of p38 γ as a therapeutic target in HCC, opening a new avenue in the fight against this incurable disease.

References

- 1 Malumbres, M. Cyclin-dependent kinases. *Genome Biol* **15**, 122 (2014).
- 2 Varjosalo, M. *et al.* The protein interaction landscape of the human CMGC kinase group. *Cell reports* **3**, 1306-1320, (2013).
- 3 Malumbres, M. & Barbacid, M. Cell cycle, CDKs and cancer: a changing paradigm. *Nature reviews. Cancer* **9**, 153-166, (2009).
- 4 Canhoto, A. J., Chestukhin, A., Litovchick, L. & DeCaprio, J. A. Phosphorylation of the retinoblastoma-related protein p130 in growth-arrested cells. *Oncogene* **19**, 5116-5122, (2000).
- 5 Mayhew, C. N. *et al.* Liver-specific pRB loss results in ectopic cell cycle entry and aberrant ploidy. *Cancer research* **65**, 4568-4577, (2005).
- 6 Gubern, A. *et al.* The N-Terminal Phosphorylation of RB by p38 Bypasses Its Inactivation by CDKs and Prevents Proliferation in Cancer Cells. *Molecular cell* **64**, 25-36, (2016).
- 7 Sabio, G. *et al.* p38gamma regulates the localisation of SAP97 in the cytoskeleton by modulating its interaction with GKAP. *The EMBO journal* **24**, 1134-1145, (2005).
- 8 Gonzalez-Teran, B. *et al.* p38gamma and delta promote heart hypertrophy by targeting the mTOR-inhibitory protein DEPTOR for degradation. *Nature communications* **7**, 10477, (2016).
- 9 Gonzalez-Teran, B. *et al.* Eukaryotic elongation factor 2 controls TNF-alpha translation in LPS-induced hepatitis. *The Journal of clinical investigation* **123**, 164-178, (2013).
- 10 Lundberg, A. S. & Weinberg, R. A. Functional inactivation of the retinoblastoma protein requires sequential modification by at least two distinct cyclin-cdk complexes. *Molecular and cellular biology* **18**, 753-761 (1998).
- 11 Hu, W. *et al.* Concurrent deletion of cyclin E1 and cyclin-dependent kinase 2 in hepatocytes inhibits DNA replication and liver regeneration in mice. *Hepatology* **59**, 651-660, (2014).
- 12 Narasimha, A. M. *et al.* Cyclin D activates the Rb tumor suppressor by mono-phosphorylation. *eLife* **3**, (2014).
- 13 Diril, M. K. *et al.* Cyclin-dependent kinase 1 (Cdk1) is essential for cell division and suppression of DNA re-replication but not for liver regeneration. *Proceedings of the National Academy of Sciences of the United States of America* **109**, 3826-3831, (2012).
- 14 Diskin, R., Askari, N., Capone, R., Engelberg, D. & Livnah, O. Active mutants of the human p38alpha mitogen-activated protein kinase. *The Journal of biological chemistry* **279**, 47040-47049, (2004).
- 15 Giacinti, C. & Giordano, A. RB and cell cycle progression. *Oncogene* **25**, 5220-5227,

- (2006).
- 16 Repetto, M. V. *et al.* CDK and MAPK Synergistically Regulate Signaling Dynamics via a Shared Multi-site Phosphorylation Region on the Scaffold Protein Ste5. *Molecular cell* **69**, 938-952 e936, (2018).
 - 17 Manieri, E. & Sabio, G. Stress kinases in the modulation of metabolism and energy balance. *Journal of molecular endocrinology* **55**, R11-22, (2015).
 - 18 Hui, L. *et al.* p38alpha suppresses normal and cancer cell proliferation by antagonizing the JNK-c-Jun pathway. *Nature genetics* **39**, 741-749, (2007).
 - 19 Matesanz, N. *et al.* p38alpha blocks brown adipose tissue thermogenesis through p38delta inhibition. *PLoS biology* **16**, e2004455, (2018).
 - 20 Gonzalez-Teran, B. *et al.* p38gamma and p38delta reprogram liver metabolism by modulating neutrophil infiltration. *The EMBO journal*, (2016).
 - 21 Postic, C. & Magnuson, M. A. DNA excision in liver by an albumin-Cre transgene occurs progressively with age. *Genesis* **26**, 149-150 (2000).
 - 22 Trakala, M. *et al.* Functional reprogramming of polyploidization in megakaryocytes. *Dev Cell* **32**, 155-167, (2015).
 - 23 Cubero, F. J. *et al.* Haematopoietic cell-derived Jnk1 is crucial for chronic inflammation and carcinogenesis in an experimental model of liver injury. *Journal of hepatology* **62**, 140-149, (2015).
 - 24 Zheng, K., Cubero, F. J. & Nevzorova, Y. A. c-MYC-Making Liver Sick: Role of c-MYC in Hepatic Cell Function, Homeostasis and Disease. *Genes (Basel)* **8**, (2017).
 - 25 Askari, N. *et al.* Hyperactive variants of p38alpha induce, whereas hyperactive variants of p38gamma suppress, activating protein 1-mediated transcription. *The Journal of biological chemistry* **282**, 91-99, (2007).
 - 26 Miao, C. H. *et al.* Inclusion of the hepatic locus control region, an intron, and untranslated region increases and stabilizes hepatic factor IX gene expression in vivo but not in vitro. *Molecular therapy : the journal of the American Society of Gene Therapy* **1**, 522-532, (2000).
 - 27 Case, D. A. *et al.* *AMBER 12*, University of California, San Francisco, 2012.
 - 28 Hamelberg, D., Mongan, J. & McCammon, J. A. Accelerated molecular dynamics: A promising and efficient simulation method for biomolecules. *J. Chem. Phys.* **120**, 11919-11929, (2004).
 - 29 Hamelberg, D., Oliveira, C. A. F. d. & McCammon, J. A. Sampling of slow diffusive conformational transitions with accelerated molecular dynamics. *J. Chem. Phys.* **127**, 155102, (2007).

ACKNOWLEDGEMENTS

We thank S. Bartlett for English editing, Dr D. Engelberg for the constitutively-active mutants, Division of Signal Transduction Therapy (DSTT), for recombinant proteins and CNIC Advanced Imaging and Vector Units for technical support. G.S. (RYC-2009-04972), F.J.C (RYC-2014-15242), Y.A.N (RYC-2015-17438) and S.O (RYC-2014-16846) are investigators of the Ramón y Cajal Program. E.M and M.T. was awarded La

Caixa fellowship and R. R-B. Fundación Ramón Areces-UAM fellow. B.G.T FPI Severo Ochoa CNIC program (SVP-2013-067639). This work was funded by grants supported in part by funds from European Regional Development Fund (ERDF): to G.S. European Union's Seventh Framework Programme (FP7/2007-2013) ERC 260464, EFSD/Lilly European Diabetes Research Programme Dr Sabio, 2017 Leonardo Grant for Researchers and Cultural Creators, BBVA Foundation (Investigadores-BBVA-2017) IN[17]_BBM_BAS_0066, MINECO-FEDER SAF2016-79126-R, and Comunidad de Madrid IMMUNOTHERCAN-CM S2010/BMD-2326 and B2017/BMD-3733; A.T-L Juan de la Cierva and MINECO SAF2014-61233-JIN; F.F.: European Community for MSCA-IF-2014-EF-661160-MetAcembly grant. S.O.: Spanish MINECO CTQ2014-59212-P, European Community for CIG project (PCIG14-GA-2013-630978), and European Research Council (ERC) under the European Union's Horizon 2020 (ERC-2015-StG-679001-NetMoDEzyme). Y.A.N.: German Research Foundation (SFB/TRR57/P04 and DFG NE 2128/2-1), the MINECO SAF2017-87919R; F.J.C. EXOHEP-CM S2017/BMD-3727 and the COST Action CA17112.; F.J.C. MINECO SAF2016-78711, the AMMF Cholangiocarcinoma Charity 2018/117. F.J.C. Gilead Liver Research Scholar. M. Malumbres: MINECO (SAF2015-69920-R cofunded by ERDF-EU), Consolider-Ingenio 2010 Programme (SAF2014-57791-REDC), Excellence Network CellSYS (BFU2014-52125-REDT), the iLUNG Programme (B2017/BMD-3884) from the Comunidad de Madrid. J. Bravo MINECO SAF2015-67077-R and SAF2017-89901-R. J.V MINECO (BIO2015-67580-P), the Carlos III Institute of Health-Fondo de Investigación Sanitaria (ProteoRed PRB3, IPT17/0019 - ISCIII-SGEFI / ERDF), Fundación La Marato and "La Caixa" Banking Foundation (HR17-00247). M.Marcos. ISCIII and FEDER PI16/01548 and Junta de Castilla y León GRS

1362/A/16 and INT/M/17/17; to J.L.-T.T. Junta de Castilla y León GRS 1356/A/16 and GRS 1587/A/17; JRC MCNU (SAF2017-84494-C2-1-R). The CNIC is supported by the Ministerio de Ciencia, Innovación y Universidades (MCNU) and the Pro CNIC Foundation, and is a Severo Ochoa Center of Excellence (SEV-2015-0505)

Author Contributions

G.S. conceived, and supervised this project. G.S and A. T-L designed, developed the hypothesis. E.M, L. L-V, M L and A. T-L performed DEN, CCl₄, STZ, DSS experiments, A. T-L analyzed the data. B. G-T, A. T-L, A.M performed PHx. A. M, A. S, R. R-B and A. T-L figures 2a, 2a. A. T-L, H.M and B. C: cells experiments. A P-C performed S10b. E. R, A P-C, A. C. Immunostaining and A. T-L analyzed the data. M. Malumbres, M.T, A. M, A. S, V. M-R and A. T-L CDK2 KO experiments. M. Marcos, L. H-C, O. B, J.L. T, N. M. Human analysis. Y, A-N, F. J-C and R. R-B genetic HCC models. S.O and F. F: Molecular dynamics. J. A. B and M. R-M generated the AAVs. J. B: Heuristic three-dimensional analysis. J.A.L and J. V performed and analyze the proteomic. J. R-C: MRI, A. T-L analyzed the data. D M-S Phylogenetic tree. A. T-L, performed the rest of experiments. A. T-L and G.S. wrote the manuscript with input from all authors.

*To whom correspondence should be addressed:

Guadalupe Sabio, DVM, PhD.

Assistant Professor

Centro Nacional de Investigaciones Cardiovasculares

C/ Melchor Fernández Almagro, 3

28029 Madrid (Spain)

tel.: (34) 91453 12 00 ext 2004

Competing Financial Interests

The authors report no financial conflict of interest.

Data availability

The datasets supporting the findings of this study are available within the paper and its Supplementary Information. Source Data (gels and graphs) for Figs. 1–4 and Extended Data Figs. 1–10 are provided with the online version of the paper. There is no restriction on data availability.

FIGURE LEGENDS

Figure 1: p38 γ phosphorylates Rb and promotes liver proliferation after PHx.

a, Immunoprecipitation from control livers (AlbCRE mice) and AlbCRE-p38 γ mice (liver-specific p38 γ KO) treated with DEN for 48h using anti-p38 γ or IgG (control). **b**, p38 γ KO mice injected with adeno-associated virus (AAV8/9) expressing active p38 γ (p38 γ^*). Liver immunoblot. **c-g**, AlbCRE and AlbCRE-p38 γ mice 48h after PHx or SHAM procedure **c-d**, Liver immunoblot **e**, BrdU immunostaining. $n=3-7$. **f**, Ki67 immunostaining. $n=4-6$. **g**, PCNA immunoblot. **h**, Liver-to-tibia length ratio. ($n=3-8$). All quantification shown as mean \pm SEM. Comparisons were made by two-sided Student *t*-test or one-way ANOVA coupled to the Bonferroni post-test **, $P<0.01$; ***, $P<0.001$. Scale bars, 100 μ m.

Figure 2: p38 γ compensates the loss of CDK1/2.

a, WT mice subjected to PHx were sacrificed at the indicated time points. Liver lysated immunoprecipitated with anti-p38 γ . **b-d**, WT and CDK1/2 KO (AAV2/8-Cre) mice infected with or without active p38 γ (AAV p38 γ *) were subjected to PHx or SHAM. **b**, Immunoblot analysis. **c**, BrdU immunostaining. $n=4-7$ (one-way ANOVA); *, $P<0.05$. **e**, Ki67 immunostaining. $n= 3-5$ fields from AlbCRE mice 0h $n= 7$, 48h $n=7$; AlbCRE-p38 γ 0h $n=3$, 48 $n=3$; AlbCRE-p38 γ AAV p38 γ * 0h $n=3$, 48h $n=3$. (one-way ANOVA coupled to Kruskal-Wallis post-tests); *, $P<0.05$. Scale bars, 500 μ m. All quantification shown as mean \pm SEM.

Figure 3: p38 γ drives HCC development.

a, p38 γ immuno-staining in human HCC or healthy livers. Scale bar, 500 μ m. **b**, Pearson's correlation of mRNA levels in human livers ($n=107$). **c**, Kaplan-Meier survival curves of patients stratified by p38 γ expression $n=372$. **d-f**, DEN-induced HCC in 6-month-old. **d**, Arrows mark tumours. **e**, Number of tumours and **f**, Tumour size $n=5-11$. **g**, Kaplan-Meier analysis of survival $n=10-11$ ** $P<0.01$. Scale bar, 100 μ m. All quantification shown as mean \pm SEM. Comparisons were made by two-sided Student t -test, Mann Whitney U test or Mantel-Cox log-rank test

Figure 4: Pirfenidone inhibits p38 γ activity and protects against DEN-induced HCC.

a, Liver immunoblot 2 weeks after acute DEN treatment. **b**, Ki67 immunohistochemistry in pirfenidone-treated mice before PHx. $n=5-17$ (one way ANOVA); ***, $P<0.001$. **c-e**, 11 months DEN-treated mice with or without pirfenidone treatment. **c**, MRI **d**, Tumour number; total and maximum tumour volume per mouse ($n=20-13$), analysed at from MR images using OsiriX software; (Mann-Whitney test); *, $P< 0.05$. **e**, Kaplan-Meier

analysis of survival; (Mantel-Cox log-rank test); ***, $P < 0.001$; $n=9-6$. **f**, Immunoblot analysis in hepatic tumours (T) and lesion-free peritumour zones (L) in mice treated as in **d-f**. All data are mean \pm SEM.

MATERIALS AND METHODS

Study population and sample collection

Immunohistochemical staining of p38 γ was performed in liver samples from 46 patients (86.1% male, mean age: 69.2 years, standard deviation [SD]: 22.6 years) and 11 controls (36.4% male, mean age: 45.9 years, standard deviation [SD]: 14.7 years) recruited at the University Hospital of Salamanca, Spain. Patients were diagnosed with hepatocellular carcinoma by liver biopsy, and control individuals were recruited from patients who underwent laparoscopic cholecystectomy for gallstone disease and had no laboratory or histopathological evidence of other liver diseases. This study was approved by the Ethics Committee of the University Hospital of Salamanca. Need for informed consent for immunostaining analysis from stored tissue from patients with liver cancer was waived by the Ethical Committee. A portion of each liver biopsy was fixed in 10% formalin and stained with haematoxylin-eosin and Masson's trichrome for standard histopathological interpretation. Immunostaining of p38 γ was performed with an antibody from R&D (AF1347; 1:250).

For the analysis of liver mRNA levels, the study population included 2 groups. One group consisted of obese adult patients with body mass index (BMI) $\geq 35\text{kg/m}^2$ and a liver biopsy compatible with NAFLD who underwent elective bariatric surgery ($n=79$). The second group consisted of individuals with BMI $< 35\text{kg/m}^2$ who underwent

laparoscopic cholecystectomy for cholelithiasis ($n= 30$). Participants were excluded if they had a history of alcohol use disorders or excessive alcohol consumption ($>30\text{g/day}$ in men and $> 20\text{g/day}$ in women), chronic hepatitis C or B, or if laboratory and/or histopathological data showed causes of liver disease other than NAFLD. The study was approved by the Ethics Committee of the University Hospital of Salamanca and all subjects provided written informed consent to undergo liver biopsy under direct vision during surgery. All patients signed written informed consent for participation. Data were collected on demographic information (age, sex, and ethnicity), anthropomorphic measurements (BMI), smoking and alcohol history, coexisting medical conditions, and medication use. Before surgery, fasting venous blood samples were collected for determination of complete cell blood count, total bilirubin, aspartate aminotransferase (AST), alanine aminotransferase (ALT), total cholesterol, high-density lipoprotein, low-density lipoprotein, triglycerides, creatinine, glucose, and albumin. Baseline characteristics of these groups are listed in Appendix Table 2. Kaplan-Meier survival curves of patients stratified by low or high expression of p38 γ were obtained and plotted from Human Protein Atlas database.

Animal maintenance and treatments

Mice were housed in a pathogen-free animal facility under a 12 h light/dark cycle at constant temperature and humidity, and fed standard rodent chow and water *ad libitum*. For all studies, we employed p38 γ LoxP (B6.129-Mapk12tm1), p38 δ LoxP (B6.129-Mapk13tm1)²⁰, AblCRE (B6.Cg-Tg(Alb-cre)21Mgn/J)²¹ and whole body knock-out mice for p38 γ . Mice were backcrossed for at least 10 generations in C57BL/6. Cdk1-lox; Cdk2-KO mice, cMYCtg and LIKK γ KO were described previously²²⁻²⁴. Genotypes were determined by polymerase chain reaction (PCR). All experiments were performed with

males. Experiments involving animals were conducted in accordance with the Guide for the Care and Use of Laboratory Animals and approved by the CNIC Animal Care and Use Committee. Maximal tumour size permitted was 15 mm.

For long-term studies of liver tumour development and Kaplan–Meier analysis different protocols were assessed: i) 15-day-old mice received a single intraperitoneal (i.p.) injection of diethylnitrosamine (DEN; Sigma-Aldrich) dissolved in saline at a dose of 50 mg/kg body weight. Pirfenidone (CAS: 53179-13-8; eBioChem) was administrated in drinking water at 2 g/l starting at 7 months after DEN injection and continuing for 3 months. Mice in one randomly pre-assigned group were sacrificed at 1 or 6 months after DEN administration for histological and biochemical analyses. Age-matched mice in a second group were used to assess mortality. For short-term studies evaluating DEN-induced hepatic injury and compensatory proliferation, adult mice were treated with DEN by a single i.p. injection at a dose of 100 mg/kg of body weight and sacrificed 2 h later. ii) Streptozotocin was i.p. injected (60 mg/g) into mice at 1.5 days after birth. All mice were fed in HFD after weaning and histopathological studies were assessed at 27 weeks of age. iii) Carbon tetrachloride was injected i.p. in adult mice 3 times per week during 16 weeks. After the treatment, mice were sacrificed for histopathological and biochemical studies and tumour analysis.

For partial hepatectomy (PHx), adult mice were anaesthetized using a mixture of isoflurane/oxygen. Seventy percent of the liver was excised which involves removal of the medial and left lateral lobes (used for histological and biochemical analyses). Liver proliferation, regeneration and histological and biochemical analysis were performed at 48 h and 15 days after PHx.

Immunohistochemical analyses

Liver and tumour tissues were fixed with phosphate-buffered 10% formalin and embedded in paraffin. Sections of 5 μm were stained with haematoxylin and eosin (H&E) for histopathological examination. Cell proliferation was assessed by immunohistochemical staining for Ki67 (ab15580, 1:100; Abcam), BrdU (ab6326, 1:100; Abcam), and phospho-Rb (S795) (#9301, 1:100; Cell Signaling Technology).

BrdU treatment

Hepatocytes were labelled with BrdU *in vivo* 48 hours after PHx by i.p. injection of 2 mg BrdU. After 2 hours, mice were sacrificed and livers extracted. BrdU labelling was done according to the specification of the manufacturer (BD Pharmingen™ APC-BrdU Flow Kits).

Assessment of HCC by magnetic resonance imaging

Tumours were monitored by MRI using i.v. administered gadoxetate disodium (Primovist®; Bayer Healthcare) as contrast medium to enhance focal hepatic tumours. Tumour volume was measured using OsiriX software (Pixmeo, Switzerland). 3D gradient echovolumetric imaging with minimum TR/TE (3/1.5 ms), 20° flip angle and isotropic 150 μm spatial resolution, totalling 6 minutes acquisition time, were acquired around 10 minutes after Primovist injection (2 mg/kg body weight) via the tail vein. Images were acquired on an actively shielded 7 T horizontal scanner (Agilent, Santa Clara, CA) equipped with MM2 electronics, a 115/60 gradient insert coil, and a ^1H circular-polarization, transmit-receive volume coil of 35mm inner diameter and 30mm active length, built by Neos Biotec (Pamplona, Spain). Before contrast injection, each mouse was anaesthetized by inhalation of isoflurane/oxygen (2-4%) and monitored by

breathing rhythm and temperature (Model 1024, SA Instruments, NY). Animals were positioned supine on a customized bed with a built-in nose cone supplying inhalatory anaesthesia (1-2%) and kept at 35-37°C by warm airflow throughout the experiment. After sacrifice, livers were harvested, weighed, and the number of visible tumours counted macroscopically and measured with a calliper. The figure shows axial slices extracted from the 3D volume dataset. Tumours were harvested and frozen for biochemical analyses. For liver analysis, the largest lobe was fixed in formalin and embedded in paraffin. Sections were stained with H&E and examined microscopically.

Biochemical analysis

Total hepatic proteins were extracted from 30 mg frozen liver or tumour tissue using 500 µl of lysis buffer containing 50 mM Tris-HCl pH 7.5, 1 mM EGTA, 1 mM EDTA, 50 mM NaF, 1 mM sodium glycerophosphate, 5 mM pyrophosphate, 0.27 M sucrose, 1% Triton X-100, 0.1 mM PMSF, 0.1% β-mercaptoethanol, 1 mM sodium orthovanadate, 1 µg/ml leupeptin and 1 µg/ml aprotinin. Proteins were separated by SDS-polyacrylamide gel electrophoresis and transferred onto 0.2 µm nitrocellulose membranes (Bio Rad). Membranes were blotted with primary antibodies targeting p38 (#9212, 1:1000; Cell Signaling Technology), p38γ (#2307, 1:5000; Cell Signaling Technology), a previously described p38γ antibody used for IP¹⁹, phospho-p38 T180/Y182 (#921, 1:1000; Cell Signaling Technology), Rb (#9313, 1:1000; Cell Signaling Technology), phospho-Rb Ser 807/811 (#8516, 1:1000; Cell Signaling Technology), CDK2 ((78B2) #2546, 1:1000 Cell Signaling Technology), PCNA (ab1897, 1:1000; Abcam), vinculin (V4505, 1:1000; Sigma), and GAPDH (G9245, 1:1000; Sigma). Membranes were incubated with an appropriate horseradish peroxidase-conjugated secondary antibody (GE Healthcare) and developed using an enhanced chemiluminescent substrate (GE Healthcare). In western

blots each lane corresponds to a different mouse.

Hepatic, cardiac, and renal injury was assessed from the levels of serum alanine aminotransferase (ALT), aspartate aminotransferase (AST), creatine kinase (CK), creatinine, alkaline phosphatase, and total bilirubin; all measurements were performed at the CNIC Animal Facility Unit.

Kinase assay

For the competitive kinase assays to evaluate the cooperation between CDK2 and p38 γ , we used 0.5 μ g of total protein and 0.5 μ g of each kinase per reaction (Rb only, Rb+p38 γ , Rb+CDK2/cyclin A, Rb+p38 γ +CDK2/cyclin A). We added 100 μ M ATP to each reaction at 30 °C for 15 min. To find all the residues phosphorylated by CDK2 and p38 γ , we used 2 μ g of total protein and 1 μ g of each kinase per reaction (Rb only, Rb+p38 γ , Rb+CDK2/cyclin A, Rb+p38 γ +CDK2/cyclin A). We added 100 μ M ATP to each reaction at 30 °C for 60 min.

Reactions were run on ExpressPlusTM PAGE acrylamide gels from GenScript, stained, and bands corresponding to Rb were then excised and analysed by mass spectrometry to identify phosphopeptides⁸.

RNA isolation and quantitative real-time-PCR analysis

Total RNA was isolated from liver and tumour tissue with the RNeasy Mini Kit (Qiagen) with on-column DNase I digestion. RNA was quantified using a NanoDrop spectrophotometer. Complementary DNA synthesis was carried out using the High-Capacity complementary DNA Reverse Transcription Kit (Applied Biosystems). Expression of the housekeeping genes 18S and GAPDH was used for normalization. RT-qPCR was performed using Fast SYBR Green (Applied Biosystem) on a 7900HT Fast

Real-time PCR system (Applied Biosystem). Primer sequences were as follows (F. forward; R. reverse):

GAPDH F: TGAAGCAGGCATCTGAGGG

GAPDH R: CGAAGGTGGAAGAGTGGGA

18s F: CAGCTCCAAGCGTTCCTGG

18s R: GGCCTTCAATTACAGTCGTCTTC

CycD1 F: GGTCCATAGTGACGGTCAGGT

CycD1 R: -GCGTACCCTGACACCAATCTC

CycE F: GCCTTCACCATTTCATGTGGAT

CycE R: TTGCTGCGGGTAAAGAGACAG

CycA1 F: GTGGCTCCGACCTTTCAGTC

CycA1 R: CACAGTCTTGTC AATCTTGGCA

Rb1 F: CCGTTTTTCATGCAGAGACTAAA

Rb1 R: GAGGTATTGGTGACAAGGTAGGA

CDK1 F: AGAAGGTACTTACGGTGTGGT

CDK1 R: GAGAGATTTCCCGAATTGCAGT

CDK2 F: CCTGCTCATT AATGCAGAGGG

CDK2 R: GTGCTGGGTACACACTAGGTG

CDK4 F: ATGGCTGCCACTCGATATGAA

CDK4 R: TCCTCCATTAGGAACTCTCACAC

hCOL1A F: GAGGGCCAAGACGAAGACATC

hCOL1A R: CAGATCACGTCATCGCACAAC

Cell lines and proliferation and transfection assays

Hepatocellular carcinoma (HCC) cell lines derived from human patients (HepG2, Huh7, Snu354, Snu398 and Snu449, NCBI Biosample) and wild-type human hepatocytes (HepaRG from Life Technologies). We first studied p38 γ expression in cells derived from HCC patients to avoid the unjustified use of mice. Cell lines were tested for mycoplasma contamination by PCR. Cells were cultured in DMEM (Sigma, D5796) supplemented with 10% FBS (HyClone, SV30160.03), L-glutamine (Lonza, 20mM in 0.85% NaCl) and penicillin/streptomycin (Lonza, DE17-602E; 10000 units of each antibiotic).

HepG2 and Snu398 cells were used for knock-down assays. shRNAs against p38 γ were purchased from Dharmacon (V3LHS_636283 and V3LHS_636282).

To measure proliferation, HepG2 and Snu398 cells treated with shp38 γ or shScramble were seeded in 24-well plates at 15×10^4 cells/well at different FBS concentrations (0.1%, 0.2%, 2%, and 20%). Cells were counted after 48 hours of incubation.

For colony formation assays, 2×10^3 HepG2 and Snu398 treated with shp38 γ or shScramble were seeded in a p100 Petri dish. After 2 weeks (without changing the medium) the colonies were fixed and stained with 0.1% crystal violet.

For soft agar assays, HepG2 shp38 γ and HepG2 shScramble cells (10^5) were seeded in a p100 Petri dish between a base agar layer (0.5% agar, $1 \times$ DMEM and 10% FBS) and a

top agarose solution (0.7% agar, $1 \times$ DMEM and 20% FBS). The medium was replenished every 3 days. After 20 days, plates were stained with 0.5% crystal violet, and colonies were counted using a light microscope.

HA-Rb WT and HA-Rb Δ CDK plasmids (Addgene: 58905 and 58906 respectively) were transfected into HEK 293T cells using the calcium phosphate transfection method. Cells were lysed 36 hours post-transfection, and immunoprecipitation assays were performed.

Lentivirus and adeno-associated virus production

Lentiviruses were produced as described⁴. Transient calcium phosphate co-transfection of HEK-293T cells was carried out with shCDK1 (RMM4532-EG12534), shCDK2 (RMM4532-EG12534), shCDK4 (RMM4532-EG12567) or CDK6 (RMM4532-EG12571) from Dharmacon, together with p Δ 8.9 and pVSV-G packaging plasmids. Supernatants containing the lentiviral particles were collected 48 and 72 hours after removal of the calcium phosphate precipitate, centrifuged at $700 \times g$ at 4 °C for 10 minutes, and concentrated ($\times 165$) by ultracentrifugation for 2 hours at $121,986 \times g$ at 4 °C (Ultraclear Tubes, SW28 rotor and Optima L-100 XP Ultracentrifuge; Beckman). Viruses were resuspended in cold sterile PBS and titrated by qPCR.

AAV plasmids were cloned and propagated in the Stbl3 *E. coli* strain (Life Technologies). pCEFL Flag p38 γ D129A and pCEFL-p38 α -D176AF327S²⁵ were cloned into a liver-specific HRC-hAAT promoter plasmid²⁶ to generate pAAV-HRC-hAAT-p38 γ act (AAVp38 γ *). AAV2/8-CAG-Cre-WPRE was obtained from Harvard University. These AAV plasmids were packaged into AAV-9 or AAV-8 capsids to specifically target the liver, produced by the Viral Vector Unit (CNIC) as described⁸. Adeno-associated viruses (serotypes AAV8 and AAV9) were produced in HEK-293T cells and collected

from the supernatant. Mice were injected in the tail vein with 1×10^{11} adenoviral particles suspended in PBS.

Computational Methods. Molecular Dynamics Simulations

Molecular Dynamics simulations (MD) were used to study the spontaneous binding of the inhibitor RO3306 to the ATP-binding sites of p38 γ , CDK1, CDK2, and p38 α . The spontaneous binding of the inhibitor pirfenidone to the p38 γ ATP-binding site was also studied. The parameters for RO3306 and pirfenidone in the MD simulations were generated within the ANTECHAMBER module of AMBER 16²⁷ using the general AMBER force field (GAFF), with partial charges set to fit the electrostatic potential generated at the HF/6-31G(d) level by the RESP model. The charges were calculated according to the Merz-Singh-Kollman scheme using Gaussian 09.

Many crystal structures are available for the homologues p38 α and p38 β . However, p38 γ has only been crystallized in the phosphorylated state and in the presence of an ATP derivative in the ATP-binding site (Protein Data Bank (PDB) accession number 1CM8). In this crystal structure, the loops corresponding to residues 34-39, 316-321, and 330-334 were not resolved. For the MD simulations, we generated two models of p38 γ using the SwissModel homology model server and 1CM8 (phosphorylated and ATP-bound state p38 γ) and 3GP0 (inhibitor-bound state of p38 β) as templates. MD simulations of CDK1 were carried out using PDB 5HQ0 as a reference, removing the crystallized ligand occupying the ATP-binding site. MD simulations of CDK2 were performed using PDB 3PXR, corresponding to the *apo* CDK2 state. For p38 α , PDB 3GI3 was used as a reference for starting the MD simulations, removing the crystallized ligand occupying the ATP-binding site. In all cases, we placed RO3306 or pirfenidone in an arbitrary position

in the solvent region (more than 20 Å far from the ATP-binding site). From these coordinates, we began unrestrained conventional MD simulations (250 ns) followed by accelerated MD simulations (1500 ns for p38 γ with RO3306, 2000 ns for CDK1 with RO3306, 2250 ns for CDK2 with RO3306, 2000 ns for p38 α with RO3306, and 2000 ns for p38 γ with pirfenidone) to allow the inhibitor to diffuse freely until it spontaneously associated with the protein surface, and finally targeted the ATP-binding site. Inhibitor binding was monitored throughout the MD simulations by plotting a selected distance between the hydrogen bond acceptor of the inhibitor and the backbone of a residue located at the ATP-binding site responsible for the recognition and stabilization of the inhibitor (Met105 for p38 γ and p38 α , and Leu83 for CDK1 and CDK2; see Extended Fig. 1 and 10). Short distances indicate binding of RO3306 in the ATP-binding site. Spontaneous binding to p38 γ was observed in 5 out of 10 simulations (light purple, light and dark blue, light red, and teal in extended Fig. 1b); in the case of CDK1, spontaneous binding was observed in 2 out of 10 simulations (light blue and light pink). When binding occurs, RO3306 remains in the ATP-binding pocket for the rest of the MD simulation, thus indicating the strong affinity of the inhibitor towards p38 γ and CDK1. In contrast, spontaneous binding does not occur in p38 α or only in 1 out of 10 simulations in CDK2 (see extended Fig. 1c). Comparison of the observed spontaneous binding events in 500 ns of aMD simulation time for p38 γ and p38 δ indicate that RO3306 has a higher affinity towards p38 γ (19.7 % and 5.5% of the simulation time RO3306 is bound p38 γ and p38 δ , respectively, see extended Fig. 1d).

Each system was immersed in a pre-equilibrated truncated octahedral box of water molecules with an internal offset distance of 10 Å, using the LEAP module. All systems were neutralized with explicit counterions (Na⁺ or Cl⁻). A two-stage geometry

optimization approach was performed. First, a short minimization was made of the water molecule positions, with positional restraints on solute by a harmonic potential with a force constant of $500 \text{ kcal mol}^{-1} \text{ \AA}^{-2}$. The second stage was an unrestrained minimization of all the atoms in the simulation cell. The systems were then gently heated through six 50 ps steps, each increasing the temperature by 50 K (0-300 K) under constant-volume and using periodic-boundary conditions and the particle-mesh Ewald approach to introduce long-range electrostatic effects. For these steps, an 8 \AA cutoff was applied to Lennard-Jones and electrostatic interactions. Bonds involving hydrogen were constrained with the SHAKE algorithm. Harmonic restraints of 10 kcal mol^{-1} were applied to the solute, and the Langevin equilibration scheme is used to control and equalize the temperature. The time step was kept at 2 fs during the heating stages, allowing potential inhomogeneities to self-adjust. Each system was then equilibrated for 2 ns with a 2 fs timestep at a constant 1 atm pressure. Finally, a 250 ns conventional MD trajectory at constant volume and temperature (300 K) was collected, followed by ten replicas of 1500 ns of dual-boost accelerated Molecular Dynamics (aMD)^{28,29} for p38 γ in the presence of RO3306, ten replicas of 2000 ns of aMD for CDK1 in the presence of RO3306, ten replicas of 2250 ns of aMD for CDK2 in the presence of RO3306, ten replicas of 2000 ns of aMD for p38 α in the presence of RO3306, and five replicas of 2000 ns of aMD for p38 γ in the presence of pirfenidone. Gathering a total of 15 μs of aMD for p38 γ , 20 μs of aMD for CDK1, 22.5 μs of aMD for CDK2, and 20 μs of aMD for p38 α , all of them with RO3306, and 10 μs of aMD for p38 γ with pirfenidone. These long timescale unconstrained aMD simulations were performed with the aim of capturing a number of spontaneous binding events. aMD enhances the conformational sampling of biomolecules by adding a non-negative boost potential to the system when the system

potential is lower than a reference energy:

$$V_{\text{modified}} = \begin{cases} V_{\text{original}} - E_{\text{ref}} & \text{if } V_{\text{original}} > E_{\text{ref}} \\ 0 & \text{if } V_{\text{original}} \leq E_{\text{ref}} \end{cases} \quad (1)$$

where V_{original} is the original potential, E_{ref} is the reference energy, and V_{modified} is the modified potential.

In the simplest form, the boost potential, V_{boost} , is given by

$$V_{\text{boost}} = \alpha (V_{\text{original}} - E_{\text{ref}}) \quad (2)$$

where α is the acceleration factor. As the acceleration factor α decreases, the energy surface is flattened more and biomolecular transitions between the low-energy states are increased.

Here, a total boost potential is applied to all atoms in the system in addition to a more aggressive dihedral boost, *i.e.*, $(E_{\text{dihed}}, \alpha_{\text{dihed}}; E_{\text{total}}, \alpha_{\text{total}})$, within the dual-boost aMD approach. The acceleration parameters used in this study are as follows:

$$\begin{aligned} E_{\text{dihed}} &= V_{\text{dihed_avg}} + 3.5 \times N_{\text{res}}, \alpha_{\text{dihed}} = 3.5 \times N_{\text{res}}/5; \\ E_{\text{total}} &= V_{\text{total_avg}} + 0.2 \times N_{\text{atoms}}, \alpha_{\text{total}} = 0.2 \times N_{\text{atoms}}, \end{aligned} \quad (3)$$

where N_{res} is the number of protein residues, N_{atoms} is the total number of atoms, and $V_{\text{dihed_avg}}$ and $V_{\text{total_avg}}$ are the average dihedral and total potential energies calculated from 250 ns cMD simulations, respectively.

Data availability

The datasets supporting the findings of this study are available within the paper and its Supplementary Information. Source Data (gels and graphs) for Figs. 1–4 and Extended Data Figs. 1–10 are provided with the online version of the paper. There is no restriction

on data availability.

Statistical analysis and reproducibility

Data are expressed as means \pm SEM. Differences were analysed by Student's *t*-test, with significance assigned at *p* values <0.05 . Fisher's exact test was used to compare HCC incidence. The Wilcoxon-Mann-Whitney rank sum test was used to calculate the statistical significance of the observed differences between groups with different variances. The log-rank test was used to assess significance in the Kaplan–Meier analysis. GraphPad Prism version 5 software was used for calculations.

Animal sample size estimates were determined using power calculations. GraphPad Prism version 5 software was used for statistical analyses. Unpaired *t*-test were used to determine the power ($\alpha = 0.05$, two-tailed). We observed many statistically significant effects in the data, indicating that the effective sample size was sufficient for studying the phenomena of interest. The mice experiments were randomized. Mice were grouped based on gender (male), genotype, treatments, weight and age, and randomly selected. We were blinded to allocation during experiments and outcome assessment. For *in vivo* experiments, an investigator treated mice and collected the tissue samples. These samples were assigned code numbers. The analyses, including qPCR, immunohistochemistry staining, western blotting, were performed by another independent investigator. Experiments were repeated two to three times. All attempts at replication were successful.

Figure 1a-d, Representative of at least three independent experiments. e, Data are mean \pm SEM. *n*=3-5 fields from AlbCRE mice 0h *n*=3, 48h *n*=5; AlbCRE-p38 γ mice 0h *n*=5, 48 *n*=7 mice; ***, *P* <0.001 . Comparisons were made by one-way ANOVA

coupled to the Bonferroni post-test. **f**, Data are mean \pm SEM $n=2-5$ fields from AlbCRE mice 0h $n=4$, 48h $n=7$; AlbCRE-p38 γ mice 0h $n=4$, 48h $n=6$ mice; **, $P<0.01$; ***, $P<0.001$. Comparisons were made by one-way ANOVA coupled to the Bonferroni post-test. **g**, Representative of at least three independent experiments. **1h**, Data are mean \pm SEM. AlbCRE $n=3$, AlbCRE-p38 γ $n=8$ mice; ***, $P<0.001$. Comparisons were made by the two-sided Student *t*-test

Figure 2**a-b**, Representative of at least three independent experiments. **c**, Data are mean \pm SEM. $n= 4-5$ fields from AlbCRE 0h $n=7$, 48h $n=7$; CDK1/2 KO 0h $n=3$, 48h $n=3$; CDK1/2 KO AAV p38 γ^* 0h $n=4$, 48h $n=4$ mice; *, $P<0.05$. Comparisons were made by one-way ANOVA coupled to Kruskal-Wallis post-tests. **d**, Data are mean \pm SEM $n= 3-5$ fields from AlbCRE mice 0h $n=7$, 48h $n=7$; AlbCRE-p38 γ 0h $n=3$, 48h $n=3$; AlbCRE-p38 γ AAV p38 γ^* 0h $n=3$, 48h $n=3$; *, $P<0.05$. Comparisons were made by one-way ANOVA coupled to Kruskal-Wallis post-tests.

Figure 3**a** Immuno-histochemistry was performed in two independent experiments. **b**, Linear relationships from $n=107$ individuals tested by Pearson's correlation; $P<0.001$. **c**, Kaplan-Meier survival curves of patients stratified by low or high expression of p38 γ , $n=372$ individuals; (Mantel-Cox log-rank test); $P=3.9E^{-3}$. **e**, Data are mean \pm SEM (Mann Whitney *U* test) and **f**, (two-sided Student *t*-test) in AlbCRE $n=11$, AlbCRE-p38 γ $n=5$. **g**, Kaplan-Meier analysis of survival in DEN-treated AlbCRE $n=10$ and AlbCRE-p38 γ $n=11$ mice; (Mantel-Cox log-rank test); **, $P<0.01$.

Figure 4**a**, Representative of at least three independent experiments. **b**, Data are mean \pm SEM. AlbCre untreated 0h $n=10$; 48h $n=5$; AlbCRE-p38 γ untreated 0h $n=10$; 48h $n=7$ and AlbCre 0h $n=10$, 48h $n=10$; AlbCRE-p38 γ 0h $n=17$, 48h $n=10$ pirfenidone-

treated mice; (one way ANOVA); ***, $P < 0.001$. **c**, Representative of at least three independent experiments. **d**, Data are mean \pm SEM. Tumour number control $n=20$, Pirfenidone $n=13$; total tumour volume control $n=18$, Pirfenidone $n=13$ and maximum tumour control $n=18$, Pirfenidone $n=13$. Mann-Whitney test; *, $P < 0.05$. **e**, Kaplan-Meier analysis of survival. Mantel-Cox log-rank test; ***, $P < 0.001$; Control $n=6$, Pirfenidone-treated $n=9$ mice. **f**, Representative of at least three independent experiments. Each lane corresponds to a different liver or tumour sample.

EXTENDED DATA FIGURE LEGENDS

Extended data Figure 1: Similarities between p38s and CDKs

a, Phylogenetic tree of murine CMGC group kinases: CDK family is boxed in orange, and p38 family in green. **b-c**, Plot of the distance (in Å) between RO3306 and the ATP-binding site along the 10 accelerated MD simulations (aMD) of CDK1 and p38 γ (b), p38 α and CDK2 (c), together with representative RO3306-bound conformations. Spontaneous binding of RO3306 occurs in: 5/10 simulations in p38 γ , 2/10 in CDK1, 0/10 in p38 α , and 1/10 in CDK2. **d** Comparison of spontaneous binding events observed in 500 ns of aMD simulation time for p38 γ and p38 δ . **e**, Representative binding pathway obtained from aMD simulations of RO3306 for p38 γ and CDK1. **f**, p38 γ phosphorylation sites detected in Rb by *in vitro* kinase assay followed by mass spectrometry analysis.

Extended data Figure 2: MS analysis of *in vitro* phosphorylation of Rb by active p38 γ or CDK2/CyclinA. CDKs and Cyclins mRNA expression in AlbCRE-

p38 γ mice.

a, In an *in vitro* kinase assay, recombinant human Rb protein (2 μ g) was incubated alone or in the presence of p38 γ or CDK2/cyclinA kinases (1 μ g) and 0.2 mM of cold ATP for 60 min. The panels show interpreted MS/MS spectra demonstrating the phosphorylation of the indicated sites in Rb (in lower case letters). The table shows the total spectral counts of the peptides where each phosphosite was identified. The data are representative of at least three independent experiments. No phosphopeptides were identified in the negative control without kinase. **b**, Quantitative PCR in livers from AlbCRE and AlbCRE-p38 γ mice. Expression was normalized to GAPDH. Data are shown as mean \pm SEM ($n=15$ mice for CDK1/2/4/6 and $n=6$ mice for Cyclins A1, D1 and E1). *, $P<0.05$; **, $P<0.01$; ***, $P<0.001$. Comparisons were made by one-way ANOVA coupled to Bonferroni's post-tests.

Extended data Figure 3: Hepatocyte expression of active p38 γ reverts the liver proliferation in AlbCRE-p38 γ mice

AlbCRE control mice, AlbCRE-p38 γ mice and AlbCRE-p38 γ mice infected with AAV expressing active p38 γ (AlbCRE-p38 γ AAVp38 γ *) were subjected to two-thirds PHx or SHAM procedure. **a**, Gain liver mass, liver weight and liver/body mass ratio were measured after 15 days of PHx and expressed as the mean \pm SEM (Gain liver mass AlbCRE $n=8$ and AlbCRE-p38 γ $n=5$ mice; Liver/body weight AlbCRE $n=9$ and AlbCRE-p38 γ $n=5$ mice; Liver weight AlbCRE $n=9$ and AlbCRE-p38 γ $n=5$ mice). *, $P<0.05$; **, $P<0.01$. Comparisons were made by two-sided Student's *t*-test **b**, BrdU incorporation

quantified by cytometry. Data are mean \pm SEM ($n=3$). ***, $P<0.001$; *, $P<0.05$; **, $P<0.01$. Comparisons were made by one-way ANOVA coupled to Bonferroni's post-tests. **c**, pRb Ser795 immunostaining quantified in livers 48 hours after PHx. Representative images (left). Scale bar: 100 μ m. Data are mean \pm SEM (right) ($n=5$ mice). ***, $P<0.001$. Comparisons were made by one-way ANOVA coupled to Bonferroni's post-tests. **d**, Immunoblot analysis of liver extracts with antibodies against phospho-Rb S807/811, Rb, p38 γ , and vinculin (as a loading control), each lane corresponds to a different mouse. The data are representative of at least three independent experiments. **e**, Liver/tibia length ratio, expressed as mean \pm SEM ($n=6$ mice). *, $P<0.05$; **, $P<0.01$. Comparisons were made by one-way ANOVA coupled to Bonferroni's post-tests. **f**, Hepatocyte proliferation analysed by Ki67 immunostaining 48 hours after PHx. Representative images (left). Scale bar: 100 μ m. Ki67 positive cells, shown as mean \pm SEM (right). Comparisons were made by one-way ANOVA coupled to Kruskal-Wallis' test. **g**, WT infected with AAV expressing active p38 γ (AAVp38 γ^*) or active p38 α (AAVp38 α^*) were subjected to two-thirds PHx. Rb phosphorylation at the specified residues were assessed by western blot 48h after PHx. Antibody anti HA-tag was used as control of liver infection by AAVp38 γ^* and AAVp38 α^* , each lane corresponds to a different mouse. The data are representative of at least three independent experiments. **h**, Proliferation 48h after PHx were studied by Ki67 immunostaining (upper panel) or BrdU incorporation (lower panel) in immunohistological liver section. Scale bar: 100 μ m. Ki67 and BrdU positive cells, shown as mean \pm SEM ($n=5$ counted areas from AlbCRE 0h $n=4$, 48h $n=4$; AlbCRE-p38 γ 0h $n=3$, 48h $n=3$; AlbCRE-p38 γ AAVp38 γ^* 0h $n=3$, 48h $n=3$ mice, $n=5-25$ counted areas from WT AAVp38 γ^* $n=4$ and WT AAVp38 α^* $n=2$ mice). ***, $P<0.001$;

*, $P < 0.05$; **, $P < 0.01$. Comparisons were made by two-sided Student's *t*-test.

Extended data Figure 4: p38 δ partially compensates the lack of p38 γ .

a, Kaplan-Meier analysis of survival in PHx-treated AlbCRE and AlbCRE-p38 γ mice. $n=20$ mice per genotype. Mantel-Cox log-rank test were used. **b**, Liver Rb phosphorylation was studied in AlbCRE and AlbCRE-p38 γ mice by western blotting with the indicated antibody 48, 60 and 72h after PHx, each lane corresponds to a different mouse. **The data are** representative of at least three independent experiments. **c**, p38 δ expression was studied by RT-PCR at different time points after PHx and the increment of its expression was represented (AlbCRE $n=7$ and AlbCRE-p38 γ $n=6$ mice). Comparisons were made by two-sided Student's *t*-test. **d-h**, AlbCRE control mice and AlbCRE-p38 $\gamma\delta$ mice were subjected to two-thirds PHx or SHAM procedure and analysed after 48, 60 or 72 hours. **d**, Kaplan-Meier analysis of survival analysed by Mantel-Cox log-rank test. **e**, Immunoblot analysis of liver extracts from AlbCRE-p38 $\gamma\delta$ mice with antibodies against phospho-Rb S807/811, Rb, p38 γ , and vinculin (loading control), each lane corresponds to a different mouse. **The data are** representative of at least three independent experiments. **f-g**, Hepatocyte proliferation were analysed by **f**, BrdU incorporation (two-sided Student's *t*-test; **, $P < 0.05$) **g**, or Ki67 immunostaining (two-sided Student *t* test with Welch's correction; *, $P < 0.01$) at 48h after PHx in AlbCRE-p38 γ ($n=3$) and AlbCRE-p38 $\gamma\delta$ ($n=3$) mice. **h**, Hepatocyte proliferation by BrdU incorporation was analyse 60 and 72h post PHx in AlbCRE mice ($n=9$ at 60h and $n=7$ at 72h), AlbCRE-p38 γ ($n=6$ at 60h and 72h) and AlbCRE-p38 $\gamma\delta$ ($n=3$ at 60h and 72h) mice. Comparisons were made by one-way ANOVA coupled to Bonferroni's post-tests; ***, $P < 0.001$. Representative images (left). Scale bar: 50 μm . Ki67 and BrdU

positive cells are quantified as mean \pm SEM (right) ($n=5$ counted areas from the specified number of mice).

Extended data Figure 5: Reduced epithelial proliferation and Rb phosphorylation in the absence of p38 γ after DSS treatment.

WT and p38 γ KO mice were treated for 6 days with DSS in the drinking water. **a**, Representative images showing the shortening of the colon after DSS treatment. **b**, Immunohistochemical staining and BrdU quantification in colon tissue sections of DSS-treated WT and p38 γ KO mice. **c**, Immunohistochemical staining and phospho-Rb S795 quantification. Quantification is shown as mean \pm SEM. $n=5-10$ fields from WT H₂O $n=5$, DSS $n=7$; p38 γ KO H₂O $n=5$, DSS $n=9$ mice; **, $P<0.01$; *** $P<0.001$. Comparisons were made by one-way ANOVA couple with Bonferroni's Multiple Comparison test in b and c. Scale bar, 100 μ m. **d**, Immunoblot analysis of Rb phosphorylation in intestine, detected with the indicated antibody, each lane corresponds to a different mouse. The data are representative of at least three independent experiments.

Extended data Figure 6: p38 γ and CDKs cooperate in the induction of Rb phosphorylation and liver proliferation.

a, *In vitro* kinase assay, phosphorylation sites identified by mass spectrometry are underlined. **b**, Immunoblot analysis of CDK2 in p38 γ immunoprecipitates from liver of AlbCRE-p38 γ mice with or without infection with AAV expressing active p38 γ (AAVp38 γ^*). **c**, Immunoblot analysis of liver Rb expression in WT and CDK1/2 KO mice (AAV2/8-Cre-infected) in steady state. **d**, BrdU immunostaining analysis o after PHx. Quantification is shown as mean \pm SEM. $n=5$ fields from 0h $n=4$, 2h $n=5$, 8h $n=5$,

12h $n=5$, 24h $n=5$, 36h $n=7$, 48h $n=14$, 60h $n=6$, 72h $n=4$ mice. (one-way ANOVA couple with Bonferroni's Multiple Comparison test). **e**, Immunoblot analysis in livers from AlbCRE and AlbCRE-p38 γ mice. **f**, Immunoprecipitation–immunoblot analysis of CDK2 interaction with WT and nonphosphorylatable Rb in HEK-293T cells transfected with human HA-Rb WT or HA-Rb Δ CDK (nonphosphorylatable by CDKs). **g–m**, WT mice were injected with lentivirus containing shScramble or shRNA targeting CDK1/2 (shCDK1/2) or CDK4/6 (shCDK4/6) with or without AAV expressing active p38 γ (AAV p38 γ^*). Mice were subjected to PHx or a SHAM procedure. **g,k,l** Immunoblot analysis. Hepatocyte proliferation analysed by Ki67 immunostaining 48 hours after PHx. Scale bar, 50 μ m **h, i, m** Hepatocyte proliferation was analysed by Ki67 immunostaining 48 hours after PHx. Scale bar, 100 μ m. Ki67-positive cell quantification is shown as mean \pm SEM. **i**, ($n=5-10$ counted areas from WT 0h $n=2$, 48h $n=3$; shCDK1/2 0h $n=3$, 48h $n=4$; shCDK1/2 0h AAV p38 γ^* 0h $n=4$, 48h $n=5$ mice); ***, $P<0.001$. (one-way ANOVA couple with Bonferroni's Multiple Comparison test). **m**, ($n=5$ counted areas from $n=5$ mice). ***, $P<0.001$. Comparisons were made by two-sided Student *t* test. In the western blots, each lane corresponds to a different mouse and are representative of at least three independent experiments.

Extended data Figure 7: p38 γ expression is increased in human HCC.

a, Percentage of HCC patients with mutations in p38 γ , CDK1, and CDK2 and the number of HCC mutations in p38 γ , CDK1, and CDK2. Data were obtained from the International Cancer Genome Consortium (data from 17/07/2017). **b**, Expression of p38 γ in human primary hepatocytes and in human HCC cell lines (Huh7, HepG2, Snu449

and Snu398) or other type of cancer cells (HTB77). **c**, Immunoblot analysis of phospho-p38 γ and total p38 γ in liver extracts from mice lacking IKK γ in the liver (LIKK γ KO) and control littermates (WT) (left) and from c-MYC transgenic mice (cMYCtg) and WT counterparts (right). p38 γ phosphorylation was detected only in mice lacking IKK γ specifically in the liver or overexpressing C-MYC. Vinculin served as a loading control. In the western blots each lane corresponds to a different mouse and are representative of at least three independent experiments. **d**, Immunohistochemical staining of p38 γ in human HCC liver. Negative control, p38 γ KO mice; Positive control, p38 γ KO mice infected with human AAVp38 γ . The chart shows stratification of p38 γ expression in human liver samples as no expression, low, medium, and high expression ($n=46$ patients with HCC and $n=11$ healthy patients).

Extended data Figure 8: p38 γ expression is necessary for Snu398 and HepG2 proliferation.

a, Immunoblot analysis of Snu398 cells treated with lentiviral particles containing two p38 γ -targeting shRNAs (B5 or G1) or shScramble. Representative western blot of at least three independent experiments. **b**, Growth of Snu398 cells infected with shp38 γ or shScramble. Cells were plated and cultured for 2 days in medium supplemented with different serum concentrations. Relative cell number was measured by crystal violet staining. Data are mean \pm SEM ($n=12$). ***, $P<0.00$. Comparisons were made by two-way ANOVA. **c**, Colony formation assay of Snu398 cells infected with shp38 γ or shScramble, representative images. **d**, Cells were grown in DMEM with 10% serum. The number of colonies with >10 cells was counted after 15 days. . Data are mean \pm SEM

($n=3$) and are representative of results from three independent experiments. **, $P<0.01$, ***, $P<0.001$. Comparisons were made by two-sided Student's *t*-test. **e**, Immunoblot analysis in HepG2 cells treated with lentiviral particles containing a shRNA against p38 γ or scramble control. Representative western blot of at least three independent experiments. **f**, Growth of HepG2 cells infected with shp38 γ or shScramble. Cells were plated and cultured for 2 days in medium supplemented with different serum concentrations. Relative cell numbers were measured by crystal violet staining. Data are mean \pm SEM ($n=3$) and are representative of results from three independent experiments. ***, $P<0.001$. Comparisons were made by two-way ANOVA. **g**, Colony formation assay of HepG2 cells infected with shp38 γ or shScramble, representative images. Cells were grown in DMEM with 10% serum. The number of colonies with >10 cells was counted after 15 days. Representative images are shown. Data are mean \pm SEM ($n=3$). ***, $P<0.001$. Comparisons were made by two-sided Student's *t*-test. **h**, Soft agar assay of HepG2 cells infected with shp38 γ or shScramble. Cells were grown in DMEM with 10% serum. The number of colonies with >10 cells was counted after 20 days. Data are mean \pm SEM ($n=12$). ***, $P<0.001$. Comparisons were made by t Mann-Whitney test.

Extended data Figure 9: Alb-Cre p38 γ mice are protected against CCl₄-induced liver damage and HCC-induced by type 1 diabetes.

a, Immunoprecipitation–immunoblot analysis of phospho and total p38 γ in liver extracts from AlbCRE control mice, showing p38 γ activation upon acute DEN treatment (100 mg/kg for 2 hours). Liver lysates (2 mg) were immunoprecipitated with anti-p38 γ antibody followed by immunoblotting as indicated. **b**, Immunoblot analysis of Rb S807/811 phosphorylation and PCNA content in liver of AlbCRE mice and Alb-Cre p38 γ

mice 1 month after DEN injection. Vinculin is shown as a loading control. **c**, Representative images of Ki67 immunohistochemistry in livers of AlbCRE and Alb-Cre p38 γ mice 8 months after DEN injection. Scale bar, 500 μ m. Data are mean \pm SEM. $n=10$ fields in $n=7$ mice; (two-sided Student *t*-test); *** $P<0.001$. **d-e**, AlbCRE and Alb-Cre p38 γ mice were injected with 2 ml/kg of CCl₄ (v/v) in 20% corn oil, three times per week for 14 weeks. All mice were fed a HFD. **d**, Representative images of liver tumours (left panel) and quantification of tumour size (right panel); *** $P<0.001$; Comparisons were made by two tail Student's *t*-test with Welch's correction. **b**, Immunohistochemical staining and Ki67 quantification on liver tissue sections; *** $P<0.001$; Comparisons were made by two-sided Student's *t*-test. Scale bar, 100 μ m. Quantification is shown as mean \pm SEM. $n=5$ fields from $n=9$ mice. **c-d**, Streptozotocin was subcutaneously injected (60 mg/g) into AlbCRE and AlbCre-p38 γ mice at 1.5 days after birth. All mice were fed a HFD and histopathologically assessed at 27 weeks of age. **c**, Immunohistochemical staining for phosphor-Rb S795 on liver tissue sections (AlbCRE $n=5$, AlbCre-p38 γ $n=5$ mice); *** $P<0.001$; Comparisons were made by two tail Student's *t*-test with Welch's correction. Scale bar, 100 μ m. and **d**, Ki67 (AlbCRE $n=4$, AlbCre-p38 γ $n=5$ mice). Quantification is shown as mean \pm SEM. $n=2-6$. Scale bar, 100 μ m. ** $P<0.01$; Comparisons were made by two-sided Student's *t*-test.

Extended data Figure 10: p38 γ deletion or inhibition protects against DEN-induced HCC.

a, Upper panel, representative conformations of p38 γ and the ATP-binding site of p38 α , both with the inhibitor pirfenidone bound (in purple), extracted from the MD simulations. Central panel, activation loop is shown in teal and other relevant ATP-

binding site residues in light blue. Lower panel, plot of distance (in Å) between the oxygen of the pirfenidone carbonyl group and the amide backbone of p38 γ Met105 during the MD simulations for the 5 replicas (shown in different colours). Short distances indicate binding of pirfenidone in the ATP-binding site. Spontaneous binding of pirfenidone to p38 γ was observed in 1 out of 5 simulations. **b**, Western blot of phosphorylated Rb. 10 μ M BIRB796 or Pirfenidone for 30 min before the assay. Representative western blot of at least three independent experiments. **c**, WT mice were treated with or without pirfenidone for 10 weeks and blood concentrations of selected parameters were assayed: Alanine aminotransferase (ALT), as a readout of hepatic injury (comparisons were made by two-sided Student's *t*-test). Aspartate aminotransferase (AST), as a readout of hepatic and cardiac injury (comparisons were made by two-sided Student's *t*-test). Total bilirubin, as a readout of hepatic injury (comparisons were made by Mann Whitney test). Alkaline phosphatase, as a readout of hepatic and cardiac injury (comparisons were made by Mann Whitney test). Creatine kinase (CK) and creatinine, as a readout of cardiac and renal injury (comparisons were made by Mann Whitney test). All data are mean \pm SD ($n=10$ mice). **d**, Immunoblot analysis of p38 γ in liver and tumour samples after AAVCRE infection. Representative western blot of at least three independent experiments. **e**, Number of tumours and tumour size analysed at the end of the experiment. Data are mean \pm SEM. $n=10$ untreated and $n=20$ cre-treated mice; * $P<0.05$.; ***, $P<0.001$. (comparisons were made by two-sided Student's *t*-test with Welch's correction). **f**, Representative contrast-enhanced MRI results from mice 7 months after DEN injection with or without CRE-mediated p38 γ deletion. The figure shows axial slices extracted from the 3D volume dataset. Arrowheads mark typical liver tumours. **g**, AAVCRE mediated deletion of p38 γ protects against STZ-induced HCC.

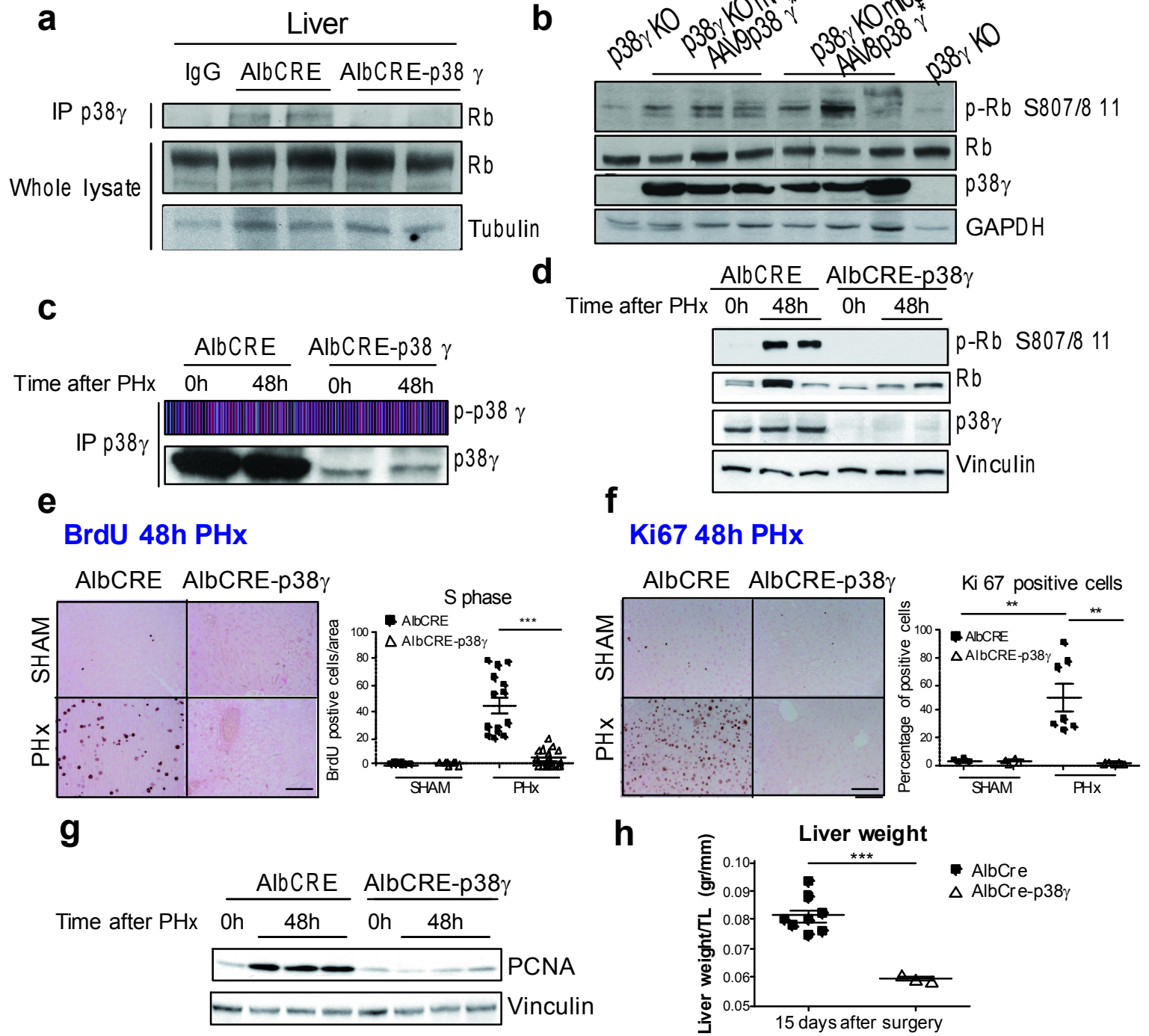
Left panel indicates increased liver damage after STZ treatment; ***, $P < 0.001$ (Comparisons were made by Student's *t*-test). Right panel shows tumour size that was analysed at the end of the experiment; *, $P < 0.05$ (Comparisons were made by one-way ANOVA coupled to the Bonferroni post-test) Data are mean \pm SEM. $n=10$ untreated and $n=20$ CRE-excinded-treated mice. In the western blots, each lane corresponds to a different mouse.

Type of file: figure

Label: 1

Filename: figure_1.ai

Figure 1

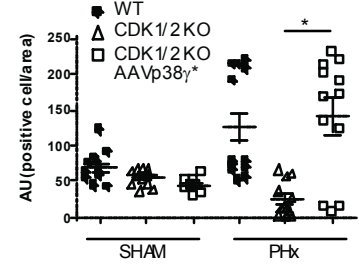
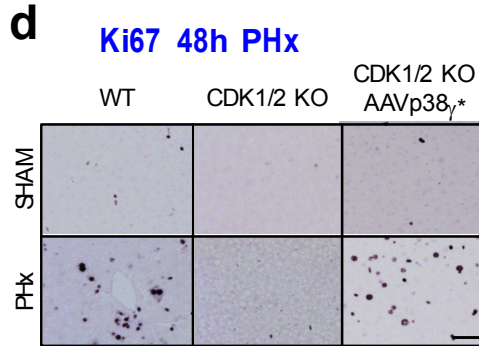
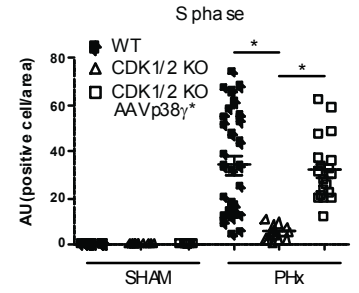
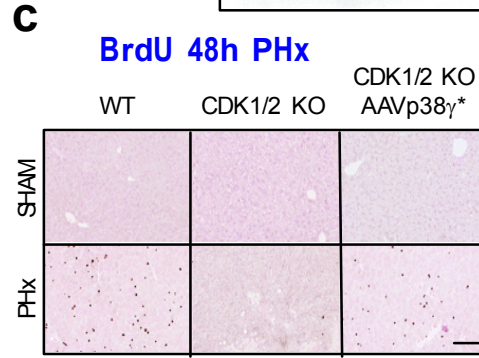
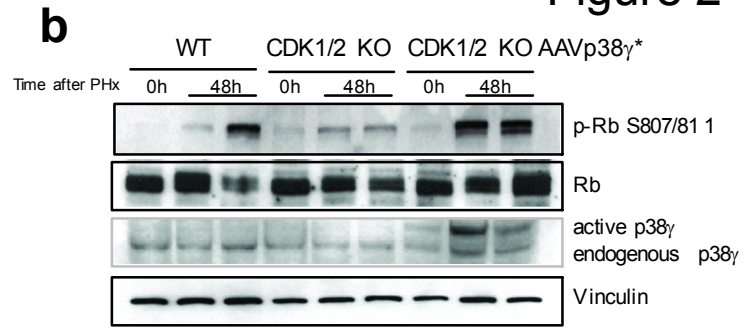
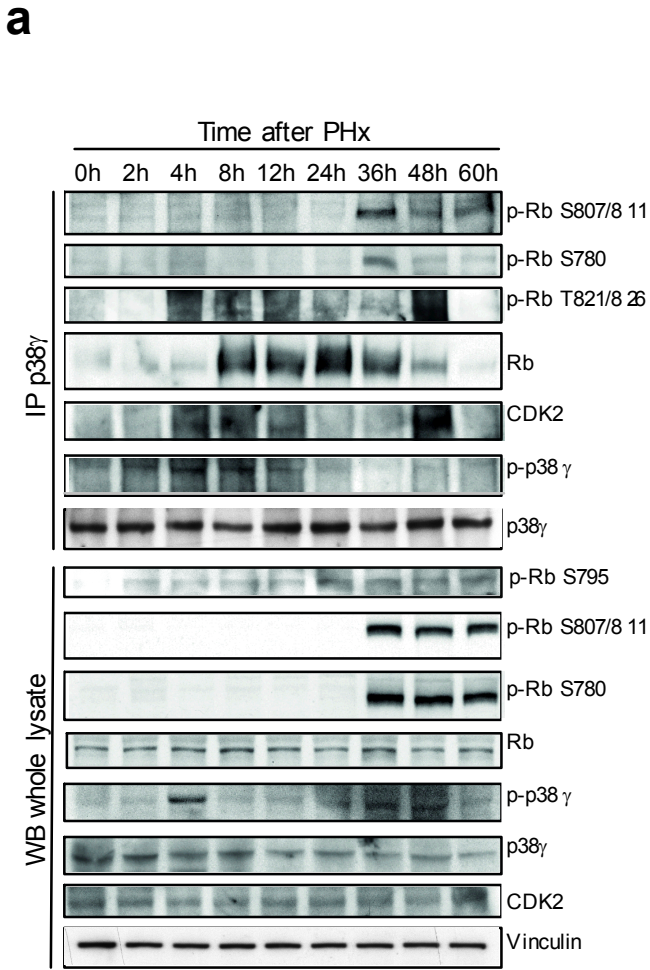


Type of file: figure

Label: 2

Filename: figure_2.ai

Figure 2



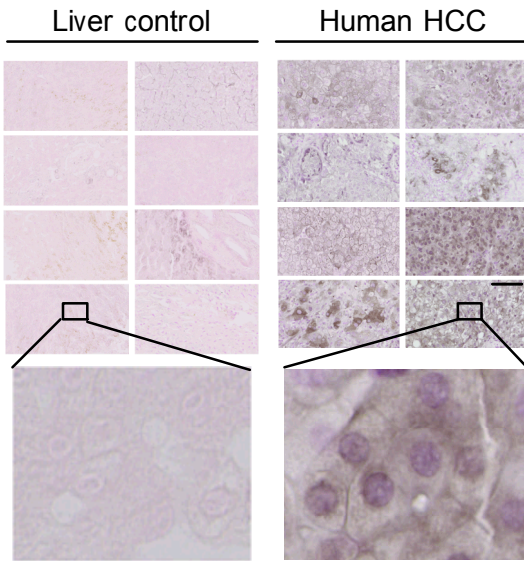
Type of file: figure

Label: 3

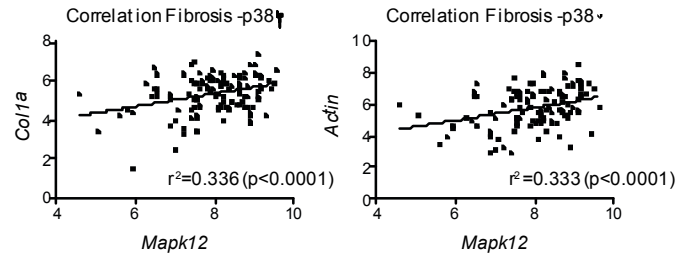
Filename: figure_3.ai

a

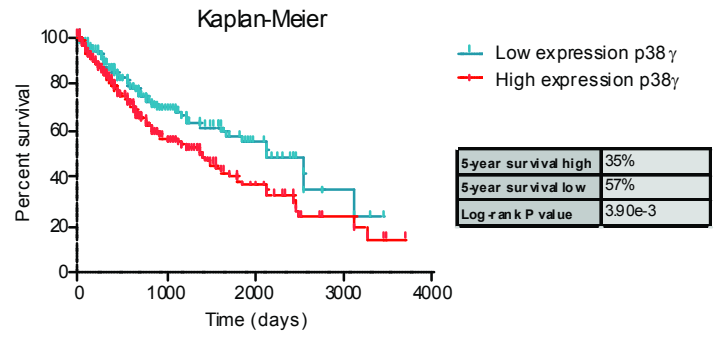
p38 γ staining



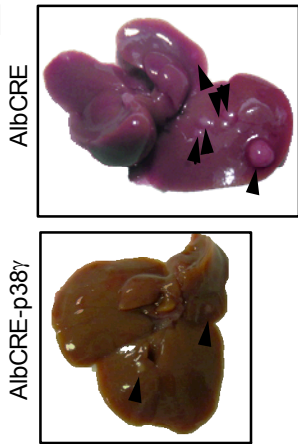
b



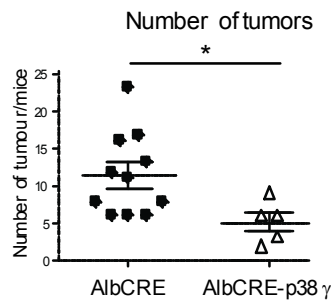
c



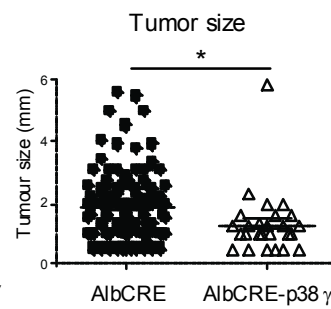
d



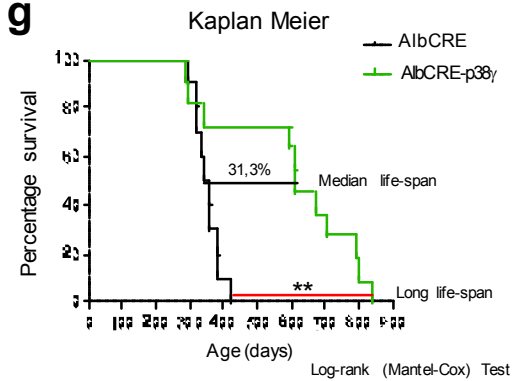
e



f



g



Type of file: figure

Label: 4

Filename: figure_4.ai

